

---

This is an electronic reprint of the original article.  
This reprint may differ from the original in pagination and typographic detail.

Asplund, Anton; Remes, Heikki; Ono, Yuki

## Modeling of Stress–Strain Fields Below U-Notch Root Using Plasticity Approximation Rules Under Variable-Amplitude Loading

*Published in:*  
Fatigue and Fracture of Engineering Materials and Structures

*DOI:*  
[10.1111/ffe.14525](https://doi.org/10.1111/ffe.14525)

Published: 01/02/2025

*Document Version*  
Publisher's PDF, also known as Version of record

*Published under the following license:*  
CC BY-NC-ND

*Please cite the original version:*  
Asplund, A., Remes, H., & Ono, Y. (2025). Modeling of Stress–Strain Fields Below U-Notch Root Using Plasticity Approximation Rules Under Variable-Amplitude Loading. *Fatigue and Fracture of Engineering Materials and Structures*, 48(2), 900-913. <https://doi.org/10.1111/ffe.14525>

---

This material is protected by copyright and other intellectual property rights, and duplication or sale of all or part of any of the repository collections is not permitted, except that material may be duplicated by you for your research use or educational purposes in electronic or print form. You must obtain permission for any other use. Electronic or print copies may not be offered, whether for sale or otherwise to anyone who is not an authorised user.

ORIGINAL ARTICLE OPEN ACCESS

# Modeling of Stress–Strain Fields Below U-Notch Root Using Plasticity Approximation Rules Under Variable-Amplitude Loading

Anton Asplund  | Heikki Remes | Yuki Ono

Department of Mechanical Engineering, School of Engineering, Aalto University, Espoo, Finland

**Correspondence:** Anton Asplund ([anton.asplund@aalto.fi](mailto:anton.asplund@aalto.fi))**Received:** 20 June 2024 | **Revised:** 5 November 2024 | **Accepted:** 8 November 2024**Funding:** This research was funded by Aalto University and the CaNeLis project (funding from Business Finland under grant no. 3409/31/2022). The financial support is gratefully acknowledged.**Keywords:** equivalent strain energy density | fatigue damage | Neuber's rule | notch stress and strain | variable-amplitude loading | Voce–Chaboche material model**ABSTRACT**

This paper evaluates the applicability of Neuber's and equivalent strain energy density (ESED) rules to predict the material response below the root of a sharp U-notch under variable-amplitude (VA) loading for crack propagation simulations. The Voce–Chaboche (V-C) combined hardening constitutive model, coupled with the above-mentioned approximation rules, is used to resolve the elasto-plastic response over a range of depths below the notch root. The response at each load reversal is extracted, and the maximum and minimum stress and strain quantities are used to evaluate fatigue damage using the Smith–Watson–Topper parameter. Results from approximation rules are compared to finite element method (FEM) at and below the notch root. Prediction accuracy varied at different points below the root depending on the size of the plastic zone, with predictions made using the original Neuber's and ESED rules being less accurate below the root. Applying stress redistribution correction to the stress field improves its accuracy below the root; however, strain values are significantly amplified as a result. A modified Neuber's rule with stress redistribution and constraint corrections predicts the distribution of the material response and fatigue damage with consistent accuracy.

**1 | Introduction**

Over the past few decades, multiscale modeling has been gaining more attention, which allows for accurate modeling of highly nonlinear localized phenomena and their effects on damage [1–4]. This can be leveraged for use in fatigue crack growth calculations to model both the crack initiation and growth phases [5, 6], using material microstructure-dependent length-scale parameters and nonlocal continuum damage mechanics. In the model of, for example, Remes [5], crack growth is modeled using the fatigue damages in process zones along the expected crack ligament line. This has been shown to predict both crack

initiation and propagation in notched members well [7, 8]. Under this approach, the fatigue crack growth rate  $da/dN$  is estimated by determining the fatigue life  $N_f$  of each process zone with size  $a_0$ , so that  $da/dN \approx a_0/N_f$ . This provides interesting alternatives to elastic–plastic fracture mechanics, which have been widely studied and successfully used in predicting fatigue crack growth; however, it requires information on the initial crack size [9–15].

To calculate crack growth rates from fatigue damages, elasto-plastic stress and strain fields surrounding a geometrical stress concentration are required and significantly impact predictions

This is an open access article under the terms of the [Creative Commons Attribution-NonCommercial-NoDerivs](https://creativecommons.org/licenses/by-nc-nd/4.0/) License, which permits use and distribution in any medium, provided the original work is properly cited, the use is non-commercial and no modifications or adaptations are made.

© 2024 The Author(s). *Fatigue & Fracture of Engineering Materials & Structures* published by John Wiley & Sons Ltd.

## Summary

- Fatigue damage distribution below notch predicted for variable-amplitude loading has been widely studied.
- Quick calculations of elasto-plastic stress and strain fields below sharp notch tip are important.
- Approximation rules combined with Voce–Chaboche (V-C) mixed hardening model are used.
- Stress redistribution correction and modified Neuber rule predict the distribution of the material response and fatigue damage with consistent accuracy.

[16]. Averaged quantities of the stress and strain fields are used to give more accurate predictions of material failure than predictions made using peak quantities [5, 17]. Approximation rules such as Neuber's rule [18] are often used to estimate the plastic response surrounding notches, as they avoid the use of time-consuming local elasto-plastic finite element method (FEM) simulations.

Neuber's rule [18] and the equivalent strain energy density (ESED) rule introduced by Molski and Glinka [19, 20] represent two classical plasticity approximation rules that have been used in engineering analysis. Neuber's rule can be simply interpreted as requiring that the products of stress and strain are equal in the pseudo-elastic (with stress and strain variables  $s, e$ ) and elasto-plastic cases (with variables  $\sigma, \epsilon$ ). The ESED rule provides an alternative approximation rule essentially requiring that the areas under the respective stress–strain curves must be equal in pseudo-elastic and elasto-plastic cases. These two approximation rules read as follows:

$$s e = \sigma \epsilon \text{ (Neuber)}, \quad (1)$$

$$\int_0^e s de = \int_0^\epsilon \sigma d\epsilon \text{ (ESED)}. \quad (2)$$

A modification of Neuber's rule was presented by Stephens et al. [21], who proposed it to consider different states of constraint between plane stress and plane strain. The modified rule employs an additional parameter  $m$  in Neuber's rule, as follows:

$$K_\epsilon K_\sigma = K_t^2 \text{ (original)}, \quad (3)$$

$$\left(\frac{K_\epsilon}{K_t}\right) \left(\frac{K_\sigma}{K_t}\right)^m = 1 \text{ (modified)}. \quad (4)$$

where  $K_t$  is the elastic stress concentration factor,  $K_\epsilon$  and  $K_\sigma$  are the plastic strain and stress concentration factors, respectively, and  $m$  is an empirical parameter ( $0 < m < 1$ ). Later studies by Wang et al. [22–24] showed that, while determining  $m$  theoretically is challenging, it can give improved predictions with e.g. experimentally determined values. Research shows that the accuracy of the Neuber and ESED rules is case-dependent and can feature significant differences in predictions compared to FEM. In general, Neuber's rule gives conservative estimates of stress and strain at the root of a notch, while the ESED rule gives nonconservative estimates at the root [25]. This observation applies to different loading cases, such as tension, torsion,

or bending loading [25]. Furthermore, the constitutive model has been shown to affect predictions [26], as coupling to a constitutive model causes it to play an integral role in stress–strain predictions. Most of these earlier studies have focused on the stress and strain behavior only at the root of a notch rather than on the stress–strain field below the notch root, which is crucial for fatigue damage and crack propagation calculations using nonlocal continuum damage mechanics.

A few studies have emerged in the past two decades regarding stress and strain behavior below a notch root using plasticity approximation rules. Neuber's rule, coupled with the Ramberg–Osgood (R-O) constitutive law, is typically used in these studies under constant-amplitude loading [16, 27, 28] to predict the entire stress and strain fields below a notch. These studies have shown that Neuber's rule becomes nonconservative below the root. When obtaining average quantities of the stress and strain fields for, for example, crack propagation calculations, this is a potential problem as the resulting fatigue damage can become nonconservative when averaged. The studies by Wang et al. [27] and Ince and Glinka [28] correct for the nonconservativeness by accounting for the redistribution of stresses under plasticity using load equilibrium arguments, which was shown to give more realistic stress field predictions. Under plasticity, the stress field redistributes itself to allow for the same load to be carried over the cross-section of the material under yielding. However, in the above studies, the response under variable-amplitude loading is not studied and must be inspected to assess the performance of the proposed ideas under realistic loading conditions. Furthermore, fatigue damages should also be investigated as stress redistribution correction can easily lead to overestimated notch strains [28] and thus errors in damage estimation.

To investigate the effect of complex loading histories on the evolution of the stress and strain fields, it is important to use a plasticity model accounting for cyclic hardening or softening [24, 29]. In the studies by Wang et al. [27] and Ince and Glinka [28], the R-O constitutive model was used as it is simple to implement along with an approximation rule. Since the R-O model assumes cyclically stabilized material behavior, it neglects, for example, cyclic hardening/softening. This is particularly important in crack propagation calculations, where both isotropic and kinematic hardening can affect subsequent crack growth, particularly after an overload [30]. Therefore, the behavior of approximation rules using combined isotropic and kinematic hardening models needs to be clarified regarding the stress and strain fields below the notch and resulting fatigue damages.

To further develop the utilization of plasticity approximation rules for crack growth analysis, this paper carries out a numerical study on how the Neuber and ESED rules behave when coupled with the combined hardening model of V-C under uniaxial variable-amplitude (VA) loading containing overloads. Focus is placed on predicting the cyclic stress and strain distributions along the crack ligament line below a notch as well as their resulting damage values, which are essential in crack growth calculations. A computational framework is developed to study a sharply notched specimen under uniaxial VA loading. The numerical study considers the use of stress correction to account for stress redistribution under plasticity, similarly

to the approaches by Wang et al. [27] and Ince and Glinka [28]. Also, the modified Neuber's rule by Stephens et al. [21] is used to study the influence of constraint correction on fatigue damage estimation.

## 2 | Framework

The computational framework is visualized in Figure 1. Like earlier studies [27, 28], a linear elastic solution is used as a starting point, but the plasticity modeling is further developed to account for combined hardening. The fundamental idea is that the V-C constitutive model is integrated into a form where the state at each load reversal is determined. The constitutive model is coupled with an approximation rule such as Neuber's / ESED rule to obtain elasto-plastic equivalent values  $\sigma_{eq}, \epsilon_{eq}$  for a notched case. These values are obtained for each material point along the crack ligament line below the surface. The method by Hoffmann and Seeger [31, 32] is then used to convert from equivalent to principal stress and strain values. This lets us obtain the maximum principal stress and strain components that are used in damage predictions using the Smith-Watson-Topper (SWT) damage parameter. Redistribution of stresses under plasticity is then accounted for by finding a stress distribution that ensures equilibrium. The above steps can be condensed as follows:

1. Calculate elasto-plastic  $\sigma_{eq}(x), \epsilon_{eq}(x)$  for each load reversal using approximation rule and constitutive model
2. Transform  $\sigma_{eq}, \epsilon_{eq}$  into  $\sigma_i, \epsilon_i (i = 1, 2, 3)$  using Hoffmann and Seeger's method [31]
3. Account for redistribution of stresses under plasticity by requiring equilibrium
4. Use crack-driving stress and strain quantities of each cycle to determine fatigue damages

The assumptions used in formulating the framework can be summarized as follows:

1. Uniaxial loading
2. Plasticity does not affect stress triaxiality
3. Stress redistribution under plasticity governed by  $\sigma_{yy}$  field

The assumptions will be described in more detail in this section, and the effects of the assumptions are studied in the results.

### 2.1 | Plasticity modeling

Wang and Rose [24] and Chaboche et al. [29] showcase the use of a V-C model which determines the material response at each load reversal coupled with Neuber's rule. The V-C model is chosen since it is a classical isotropic and kinematic hardening model featuring relative simplicity in modeling complicated hardening material behavior. The basis of this cyclic model is that the uniaxial stress  $\sigma$  can be obtained at a load reversal as [29] follows:

$$\sigma = \alpha + \kappa \cdot (R + \sigma_{y0}), \quad (5)$$

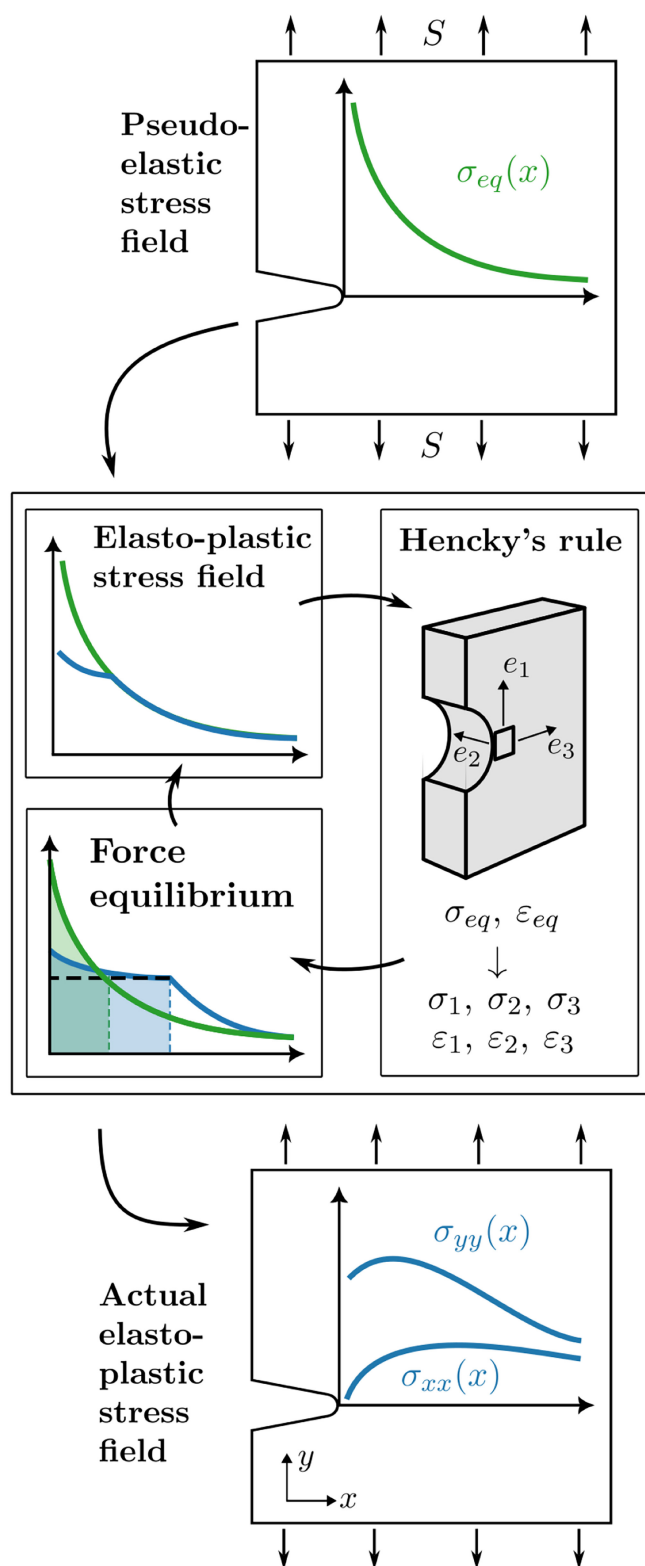


**FIGURE 1** | Visual flowchart of numerical framework used in this study. [Colour figure can be viewed at [wileyonlinelibrary.com](https://onlinelibrary.wiley.com)]

with  $\kappa = 1$  in tension and  $\kappa = -1$  in compression,  $\sigma_{y0}$  representing the von Mises equivalent nominal yield strength, with  $\alpha$  and  $R$  representing the amount of kinematic hardening and isotropic expansion, respectively. Using several backstress components  $\alpha_k$ , this becomes:

$$\sigma = \sum_{k=1}^{n_k} \alpha_k + \kappa \cdot (R + \sigma_{y0}). \quad (6)$$

The values of the backstresses  $\alpha_k$  and isotropic expansion  $R$  are commonly modeled to depend on the plastic strain  $\varepsilon_p$  present in the material, so that  $\alpha_k \rightarrow \alpha_k(\varepsilon_p)$ ,  $R \rightarrow R(\varepsilon_p)$ . Under the strain decomposition assumption,  $\varepsilon_p$  is taken as the difference between the total strain  $\varepsilon$  and the elastic strain  $\varepsilon_e$ , that is,  $\varepsilon_p = \varepsilon - \varepsilon_e$ . Explicit expressions for  $\alpha_k(\varepsilon_p)$  and  $R(\varepsilon_p)$  are then needed that can be inserted into Equation (6). The Armstrong–Frederick rule gives a differential equation for each backstress component [29]:

$$\dot{\alpha}_k(t) = [C_k - \gamma_k \alpha_k(t)] \dot{\varepsilon}_p(t), \quad (7)$$

where  $C_k$  and  $\gamma_k$  are material parameters for each backstress component  $k$ . Integrating the above from the time of the previous load reversal,  $t_0$ , to  $t$  gives after simplifying the following:

$$\alpha_k(\varepsilon_p) = \kappa \left[ \frac{C_k}{\gamma_k} - \left( \frac{C_k}{\gamma_k} - \kappa \alpha_{k,0} \right) \cdot e^{-\kappa \gamma_k (\varepsilon_p - \varepsilon_{p,0})} \right], \quad (8)$$

where quantities with a subscript of 0 denote their known value at the previous load reversal. The rate of isotropic expansion  $\dot{R}$  can also be modeled similarly as a differential equation [29]:

$$\dot{R}(t) = b[Q - R(t)] \dot{p}, \quad (9)$$

where  $Q$ ,  $b$  are material parameters and  $\dot{p}$  is the rate of accumulated plastic strain. The increment of accumulated plastic strain  $dp$  is related to the increment of the plastic strain  $d\varepsilon_p$  in the uniaxial case as  $dp = |d\varepsilon_p|$  [33]. Integrating the above similarly gives after simplification

$$R(\varepsilon_p) = Q - (Q - R_0) \cdot e^{-\kappa b (\varepsilon_p - \varepsilon_{p,0})}, \quad (10)$$

giving an expression for monotonic isotropic expansion as function of the plastic strain. For cases with a notch, coupling with an approximation rule must be performed. Neuber's rule reads as follows:

$$\varepsilon \cdot \sigma = \frac{(K_{t,eq} \cdot S)^2}{E}, \quad (11)$$

into where the expression for the actual elasto-plastic stress  $\sigma$  above, Equation (6), can be inserted. This gives a governing equation that is still a function of only one unknown,  $\varepsilon_p$ , since according to the strain decomposition assumption  $\varepsilon = \varepsilon_e + \varepsilon_p = \sigma(\varepsilon_p)/E + \varepsilon_p$ . The nominal stress  $S$  is defined as  $F/A$ , where  $F$  is the applied load over the cross-section and  $A$  the cross-sectional area at the notch. The elastic stress concentration factor of the nominal equivalent stress  $K_{t,eq}$  is used in this paper. Equation (11) then becomes

$$\left[ \frac{\sigma(\varepsilon_p)}{E} + \varepsilon_p \right] \cdot \sigma(\varepsilon_p) = \frac{(K_{t,eq} \cdot S)^2}{E}, \quad (12)$$

where according to Equation (6),

$$\sigma(\varepsilon_p) = \sum_{k=1}^{n_k} \alpha_k(\varepsilon_p) + \kappa \cdot [R(\varepsilon_p) + \sigma_{y0}]. \quad (13)$$

Coupling with an approximation rule other than Neuber's rule, such as the ESED rule, is achieved through similar arguments. During cyclic loading, Neuber's rule is recast into a form accounting for the change in quantities from one load reversal to the next [34]:

$$\Delta\varepsilon \cdot (\Delta\sigma)^m = \frac{(K_{t,eq} \cdot \Delta S)^{(m+1)}}{E}, \quad (14)$$

$$\Delta\varepsilon = \kappa(\varepsilon - \varepsilon_0), \quad (15)$$

$$\Delta\sigma = \kappa(\sigma - \sigma_0), \quad (16)$$

where  $\varepsilon_0$  and  $\sigma_0$  are quantities at the previous load reversal. The modified Neuber relation of Equation (4) is also used here. With  $m = 1$  as default ( $0 < m < 1$ ), the original Neuber's rule is recovered. This governing equation is then solved numerically using, for example, the Newton–Raphson algorithm, to obtain the stress and strain state at each load reversal. To obtain the subsurface stress and strain fields, the expressions above are applied to each inspected material point over the crack ligament line, using the values of the stress concentration factors over depth  $x$ ,  $K_{t,eq}(x)$ .

The implementation is verified in Figure 2 for a uniaxial strain-controlled case (without a notch or Neuber's rule) using S355 structural steel. Here, a VA strain-controlled load history obtained from Hartloper et al. [35] is inserted into a FEM model representing a uniaxial flat bar and the stresses are determined. Material parameters used are shown in Table 1 appearing later in Section 3. Figure 2 shows that the above implementation matches well with FEM at each load reversal.

## 2.2 | Transformation to Multiaxial Quantities

With the uniaxial stress and strain distribution obtained, the method given by Hoffmann and Seeger [31, 32] is used to transform from equivalent quantities to multiaxial quantities pertaining to a notch that are needed for damage calculations. The idea of their method is that the stress and strain states from a uniaxial simulation (here, the results obtained from using Equation (14)), are taken to instead represent equivalent quantities  $\sigma_{eq}$ ,  $\varepsilon_{eq}$ . The generalized Hooke's law is then used to solve for the principal notch stress and strain quantities. Denoted as Hencky's rule, together, the equations read [31] as follows:

$$\varepsilon_1 = \frac{\varepsilon_{eq}}{\sigma_{eq}} [\sigma_1 - \nu'(\sigma_2 + \sigma_3)], \quad (17)$$

$$\varepsilon_2 = \frac{\varepsilon_{eq}}{\sigma_{eq}} [\sigma_2 - \nu'(\sigma_3 + \sigma_1)], \quad (18)$$

$$\varepsilon_3 = \frac{\varepsilon_{eq}}{\sigma_{eq}} [\sigma_3 - \nu'(\sigma_1 + \sigma_2)], \quad (19)$$

$$\sigma_{eq} = \sqrt{\frac{1}{2} [(\sigma_1 - \sigma_2)^2 + (\sigma_2 - \sigma_3)^2 + (\sigma_3 - \sigma_1)^2]}, \quad (20)$$

## Cyclic model verification

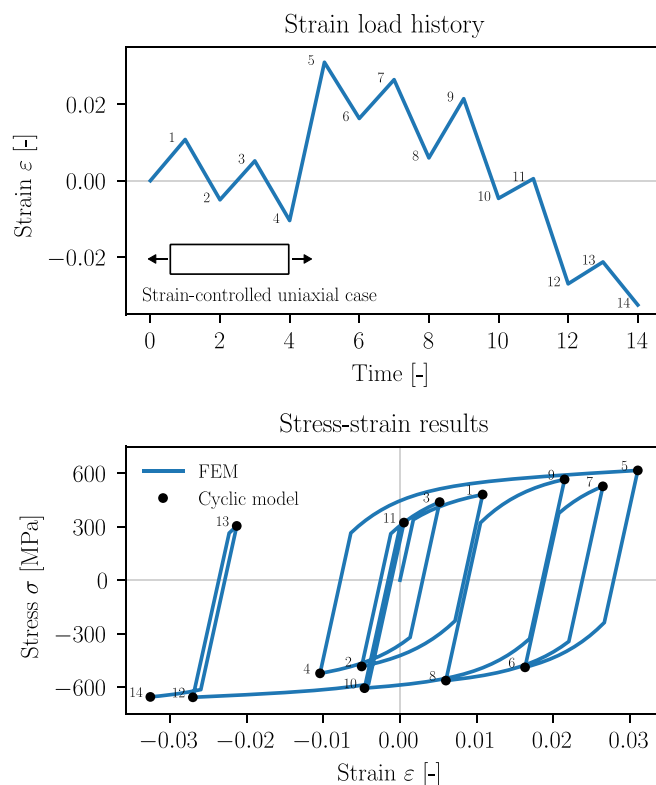


**FIGURE 2** | Verification of cyclic V-C model under strain-controlled VA load history for a uniaxial specimen. Numerical indices show associated time values. [Colour figure can be viewed at [wileyonlinelibrary.com](https://onlinelibrary.wiley.com)]

**TABLE 1** | V-C and Coffin–Manson material parameter values, from Hartloper et al. [35] and Petry [36].

$E$ (GPa)	$\sigma_{y0}$ (MPa)	$Q$ (MPa)	$b$ (-)
197.4	338.8	134.3	14.7
$C_1$ (MPa)	$\gamma_1$ (-)	$C_2$ (MPa)	$\gamma_2$ (-)
26 242.0	199.0	2 445.3	11.7
$\sigma'_{f,cm}$ (MPa)	$b_{cm}$ (-)	$\epsilon'_{f,cm}$ (-)	$c_{cm}$ (-)
887.9	-0.09	0.584	-0.56

where the directions of the principal axes are shown in Figure 1 for the special case of a simple notched specimen under uniaxial tension.  $\nu'$  is the “effective” Poisson’s ratio:

$$\nu' = \frac{1}{2} - \left( \frac{1}{2} - \nu \right) \frac{\sigma_{eq}}{E \epsilon_{eq}}. \quad (21)$$

The above is a system of four equations for six unknowns. Under plane strain, the out-of-plane strain component is zero so that  $\epsilon_2 = 0$ , leaving only one additional equation to be needed.

Hoffmann and Seeger originally presented their method specifically for the free surface of a notch where  $\sigma_3 = 0$ . However, when points below the surface along the crack ligament line are inspected, this does not hold, and additional assumptions

must be made. Here, the ratio of the in-plane stress components is set to a constant value to give an additional equation,  $\sigma_3/\sigma_1 = \text{constant}$ , which Wang et al. [27] found to be a reasonable assumption. To predict the response at locations below the root, values must be given according to some distribution of values,  $\sigma_3(x)/\sigma_1(x) = f(x)$ . For example, the analytical Creager–Paris solution [37] can be used to provide the distribution. In the case of symmetry, which is respected in the case of a fixed crack ligament line perpendicular to the notch root, the above equations can be used to obtain the crack-driving  $\sigma_{yy}$  in Cartesian coordinates.

### 2.3 | Stress Redistribution Correction

To correct the nonconservativeness of the Neuber or ESED rule below the root, redistribution of stresses under plasticity is accounted for. Figure 3 displays the underlying concept. Under a linear elastic stress distribution, a certain amount of elastic strain energy exists surrounding the notch, with more energy concentrated closer to the root. When yielding occurs, this elastic strain energy closest to the root does not fully develop. The stresses must then redistribute themselves to maintain force equilibrium. The differences between the pseudo-elastic and elasto-plastic stress distributions are shown schematically in Figure 3, displaying how the plastic boundary  $\omega_0$  predicted by the pseudo-elastic stresses increases to the actual plastic boundary  $\omega$ . To respect equilibrium, Wang et al. [27] and Glinka [38] required that the areas of the elastic

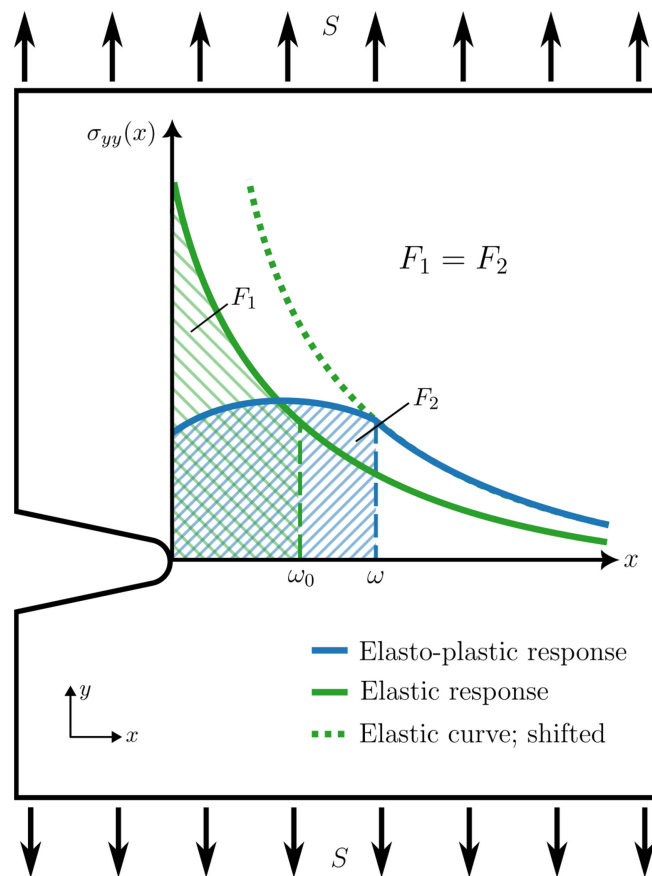


**FIGURE 3** | Schematic of the methodology behind correcting the predicted elasto-plastic stress field for redistribution of stresses occurring during plasticity. [Colour figure can be viewed at [wileyonlinelibrary.com](https://onlinelibrary.wiley.com)]

and elasto-plastic  $\sigma_{yy}(x)$  stress distributions are equal up to  $\omega_0$  and  $\omega$ , respectively. Their approach is also used in this paper.

The equivalency  $F_1 = F_2$  is solved for numerically so that first the pseudo-elastic stress distribution is amplified, with Neuber's and Hencky's rule then applied to determine the elasto-plastic  $\sigma_{yy}(x)$  distribution. Different elastic stress distributions are trialed until the condition  $F_1 = F_2$  is met. The result of this step is that the stresses in the plastic region  $0 < x < \omega$  are estimated more precisely. The stress distribution outside the plastic region is meanwhile taken to be equal to the pseudo-elastic stress distribution that has instead been shifted along  $x$  by  $\omega - \omega_0$ , shown in Figure 3 as the dotted curve.

### 3 | Numerical Study Setup

The computational framework introduced above is used to analyze a VA load case. The obtained stress and strain fields and fatigue damages resulting from the load history are compared to corresponding FEM calculations. In the current study, the elastic stress field from the FEM model is input to the computational framework instead of using, for example, the Creager–Paris solution. The FEM model provides the equivalent pseudo-elastic  $\sigma_{eq}(x)$  distribution needed to apply the approximation rule, as well as the elastic distribution of the in-plane stress components required for Hencky's rule. Since the

discrete distributions from the FEM model are used as input, the studied case essentially features the same “elements” or inspection points as the FEM model.

#### 3.1 | Numerical Setup

The geometry used in this numerical study is shown in Figure 4. A 2D plane strain plate geometry is modeled with a sharp notch resembling a short crack. The plate has a thickness of 3 mm with unit out-of-plane depth, with a 5- $\mu\text{m}$  notch root radius. The specimen choice is motivated by notch geometries that can appear in, for example, welded joints with small imperfection sizes. The FEM model is constructed in the Abaqus 2023 software featuring quarter-symmetry, to represent a double-notched specimen. Uniaxial traction is applied on the far end of the model. In the material model verification of Figure 2 (smooth specimen under strain-controlled loading), large deformations were included. However, in the subsequent case study of a notched specimen under load-controlled loading, large deformations were not included as negligible differences in results were observed (approximately 1% difference in normal strains  $\epsilon_{yy}$  at the notch root). The smallest elements at the notch root are on the order of 0.1  $\mu\text{m}$  to properly capture the traction-free  $\sigma_{xx} = 0$  condition at the notch root and to resolve the highly local gradients caused by the sharp notch employed. A generic S355 structural steel is used, with

V-C material parameters from Hartloper et al. [35] (S355J2+N 25 mm plate), as shown in Table 1.

The VA load history used is shown in Figure 5. The load history includes a main overload event of magnitude  $S_{OL} = 0.7\sigma_{y0}$  near the end of the sequence. The history is offset by  $0.1\sigma_{y0}$  to include a mean stress.

Table 2 explains the model variations used in this study. These are Neuber's rule, modified Neuber's rule, and the ESED rule, either with or without stress redistribution correction. An  $m$ -value of  $m = 0.6$  is used as an example in the variant Neuber $_{corr}^{m=0.6}$ .

### 3.2 | Results Analysis

To analyze the results, damage values are inspected in addition to stress and strain values. To obtain damage and average damage values, the SWT parameter is used, expressed as [34] follows:

$$P_{SWT} = \sigma_{max} \cdot \epsilon_{amp}, \quad (22)$$

where  $\sigma_{max}$  is the maximum value of the crack-driving stress over a closed cycle and  $\epsilon_{amp}$  is the amplitude of the corresponding strain over that same cycle. In this paper, these values correspond to  $\sigma_{yy,max}$  and  $\epsilon_{yy,amp}$ . Simple-range cycle counting according to ASTM E1049-85 [39] is used to examine how the stress-strain response of each tensile-compression pair evolves as a function of time. It is worth noting that the simple-range counting method gave results similar to those produced by the commonly accepted Rainflow counting method. The difference in damage results was between 3% and 6%. The fatigue damage is then obtained using the Coffin–Manson relation [34]:

$$P_{SWT} = \frac{(\sigma'_{f,cm})^2}{E} (2N_f)^{2b_{cm}} + \sigma'_{f,cm} \epsilon'_{f,cm} (2N_f)^{b_{cm}+c_{cm}}, \quad (23)$$

where  $\sigma'_{f,cm}$ ,  $b_{cm}$ ,  $\epsilon'_{f,cm}$ , and  $c_{cm}$  are the Coffin–Manson material parameters, with the values used in this work shown in Table 1. The number of cycles to failure  $N_f$  is solved for each cycle of the stress and strain history, and the corresponding damage is obtained as  $D = 1/N_f$ . The damages from each cycle are then summed up as per Miner's rule [34] for each “element”, to form a distribution of accumulated damage values  $D_{sum}(x)$ .

To obtain a measure of the average damage, the distribution of  $D_{sum}(x)$  over the depth below the notch root is calculated and then averaged over a certain distance. Remes et al. [5] introduced the concept of a process zone size that models the effect of the grain size in metals on fatigue crack growth. When determining fatigue damage based on quantities averaged over a certain distance, this process zone size or radius of the representative volume element (RVE),  $r_{RVE}$ , appears as an additional parameter influencing crack growth. In this study, the distribution of fatigue damage values is averaged over select  $r_{RVE}$  values to assess the impact of averaging on results. The average damage  $D_{avg}$  is defined by taking an arithmetic average over the RVE:

$$D_{avg} = \frac{1}{r_{RVE}} \sum_{x=0}^{x=r_{RVE}} D_{sum}(x). \quad (24)$$

In this study,  $r_{RVE}$  sizes relevant to S355 structural steel are employed, obtained from Remes [7]. Sizes of 2, 10, and 30  $\mu\text{m}$  are used, as shown in Table 3, along with what microstructural area they represent in welded S355 steel joints. The 2  $\mu\text{m}$  RVE size

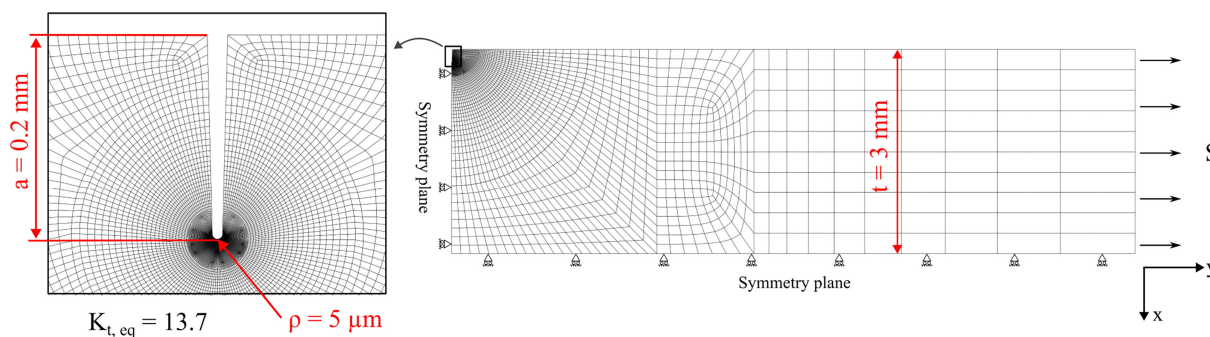


FIGURE 4 | Schematic of FEM geometry and boundary conditions. [Colour figure can be viewed at [wileyonlinelibrary.com](https://onlinelibrary.wiley.com)]

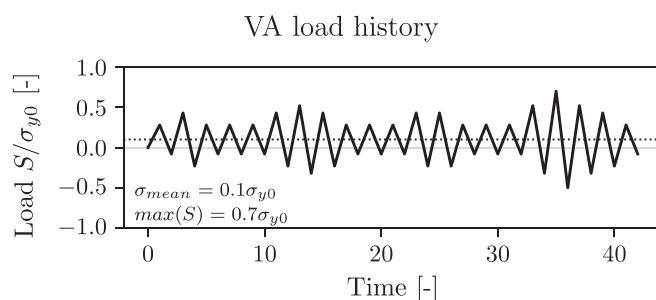


FIGURE 5 | VA load history used in this study.

approximately represents the average grain size  $d_{avg}$  in the heat-affected zone (HAZ) after welding in S355, the  $10\ \mu\text{m}$  size representing the HAZ grain size at a probability level of 99%,  $d_{99\%}$ , and  $30\ \mu\text{m}$  the  $d_{99\%}$  grain size of the base metal. These RVE sizes give relevant averaging distances that could be used in various crack propagation calculations for this material.

## 4 | Results and Discussion

### 4.1 | Monotonic Tension

Figure 6 displays the error, that is, difference between FEM and approximation rules in equivalent stress and strain distributions along the crack ligament line  $\sigma_{eq}(x)$ ,  $\epsilon_{eq}(x)$  for two monotonic

**TABLE 2** | Model variations used in this study.

Model	Stress correction	$m$ -value
Neuber	No	1.0
Neuber <sub>corr.</sub>	Yes	1.0
Neuber <sup>m=0.6</sup> <sub>corr.</sub>	Yes	0.6
ESED	No	N/A
ESED <sub>corr.</sub>	Yes	N/A

**TABLE 3** | RVE sizes  $r_{RVE}$  used in numerical study for average damage calculations; obtained from Remes [7].

Size	Location	Metric
$2\ \mu\text{m}$	HAZ	$d_{avg}$
$10\ \mu\text{m}$	HAZ	$d_{99\%}$
$30\ \mu\text{m}$	BM	$d_{99\%}$

tension load magnitudes. Errors are measured relative to FEM values, and the  $x$  axis is normalized with respect to the plastic zone size predicted by FEM,  $\omega_{FEM}$ . Both the cases with and without stress redistribution correction are shown, using the approximation rules of Neuber, modified Neuber (Equation (4) with  $m = 0.6$ ), and the ESED rule. Circular markers denote the predicted  $\omega$  values for each model variant.

As shown in Figure 6, without stress redistribution correction, the equivalent stresses are conservative at the root and become nonconservative quickly below the root. The change in slope at  $x/\omega_{FEM} \approx 0.6$  for the original Neuber and ESED rules (dashed curves) represents the edge of plasticity  $\omega_0$  as predicted by the pseudo-elastic stress distribution. This forms an area of nonconservativeness surrounding and increasing towards  $\omega_{FEM}$ . Using stress redistribution correction (solid curves) improves  $\omega$  predictions for  $S/\sigma_{y0} = 0.3$  although still causes nonconservative stress and strain distributions in certain areas below the root. Under the higher load magnitude of  $S/\sigma_{y0} = 0.7$ , however, the predictions of the plastic boundary size  $\omega$  for the stress-corrected models are not improved over the uncorrected model variants. Furthermore, while the stresses at the root are amplified to an error of approximately 15% when using correction, the strain errors become significantly conservative, with a maximum error of approximately 100%. This issue does not appear however when using also the modified Neuber's rule with  $m = 0.6$ . Since the ESED models display the same basic behavior as the Neuber models, for simplicity, only results of the Neuber models will be shown in the following VA results sections.

### 4.2 | VA Results—Stress Distributions

The crack-driving  $\sigma_{yy}(x)$  stress values are shown in Figure 7 for three different load reversals of the VA simulation: Cycle 1 tension, Cycle 1 compression, and Cycle 21 tension. Stress triaxiality  $\eta = \sigma_H/\sigma_{eq}$  values for the same time instances are also

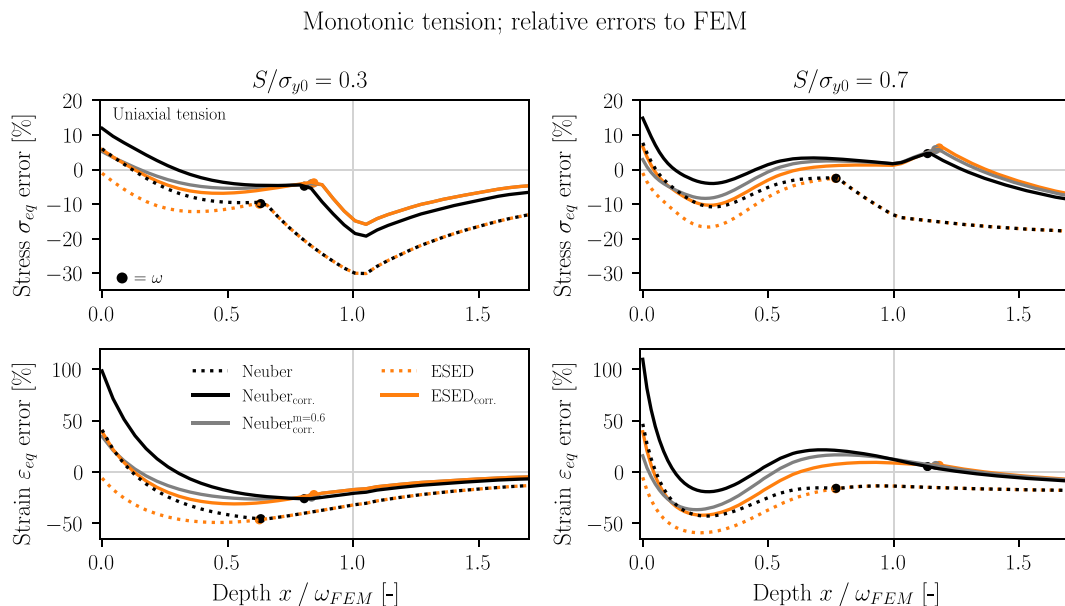


**FIGURE 6** | Equivalent stress and strain distributions,  $\sigma_{eq}$ ,  $\epsilon_{eq}$ , for a case of uniaxial monotonic tension, under two different load magnitudes. Circular markers correspond to plastic zone edge locations  $\omega$  predicted by each simulation. [Colour figure can be viewed at [wileyonlinelibrary.com](https://onlinelibrary.wiley.com)]

shown. Results are shown for the Neuber model variants (see Table 2) and are compared against FEM results.

The effect of using elastic in-plane stress component values  $\sigma_{xx}/\sigma_{yy}$  in Hencky's rule can be studied from the triaxiality values in Figure 7. Hencky's rule gives good predictions at the root, but the triaxiality values feature inaccuracies surrounding the plastic boundary  $\omega$  (vertical gray lines  $\omega_{FEM}^{tens.}$  and  $\omega_{FEM}^{compr.}$ ). It is worth noting that the triaxiality values are equal

for all Neuber cases. Stress redistribution correction does not affect triaxiality values, as they are controlled by the  $\sigma_{xx}/\sigma_{yy}$  values employed. Looking at the  $\sigma_{yy}$  values for the first load reversal, the Neuber model with stress correction deviates the most from FEM at both the root and near  $\omega$ . The deviation in  $\sigma_{yy}$  at the root is also seen from the  $\sigma_{eq}$  distribution in Figure 6, while the deviation surrounding  $\omega$  is due to the overpredicted triaxiality values when using Hencky's rule with elastic  $\sigma_{xx}/\sigma_{yy}$  values.

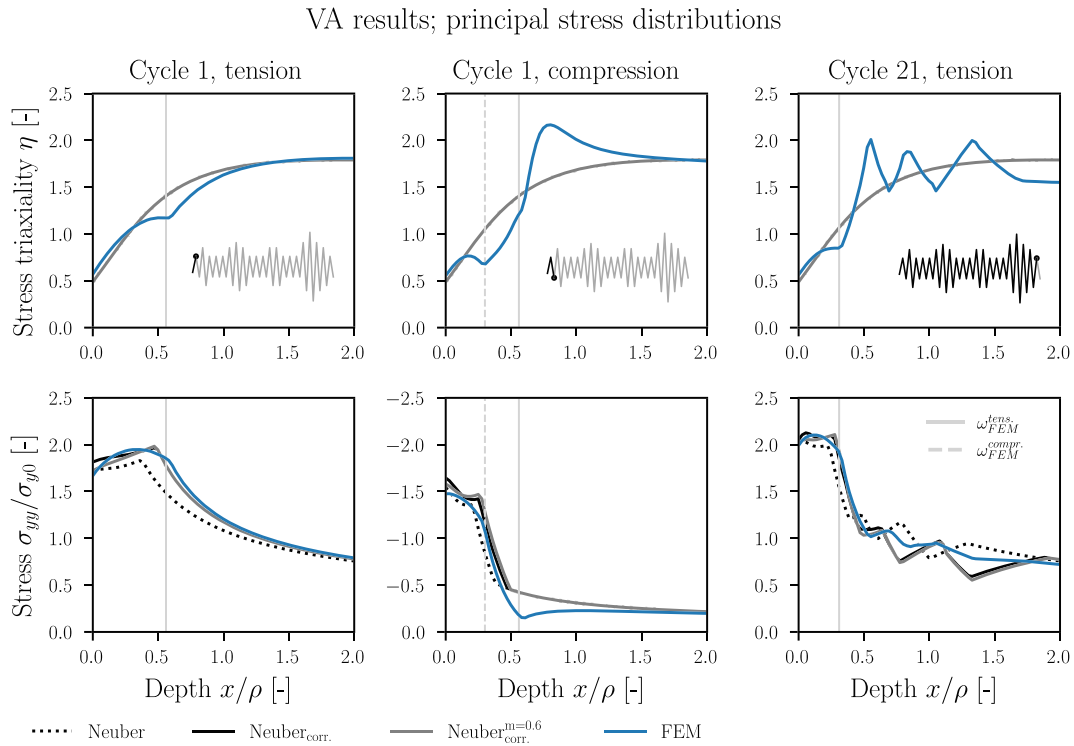


**FIGURE 7** | Distribution of triaxiality factor  $\eta$  values and  $\sigma_{yy}$  stresses for three different time instances of the VA load history. Vertical gray lines indicate plastic boundaries  $\omega$  obtained from FEM for tensile and compressive load reversals. [Colour figure can be viewed at [wileyonlinelibrary.com](https://onlinelibrary.wiley.com)]

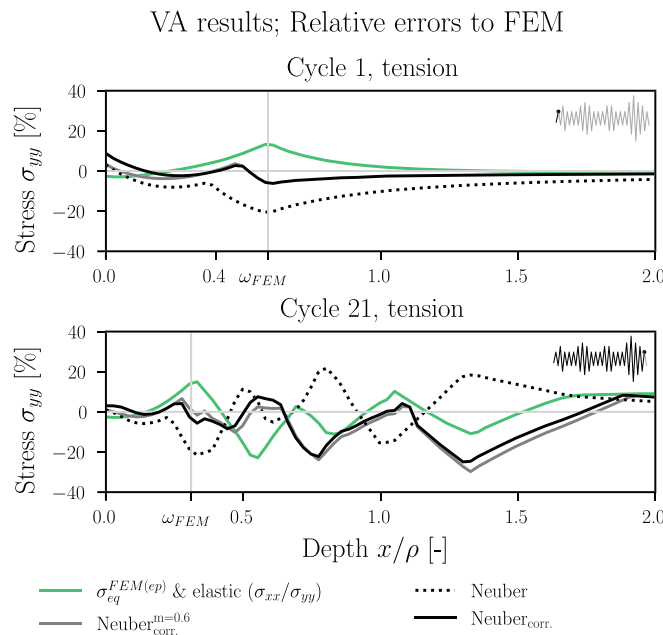


**FIGURE 8** | Relative error with respect to FEM for different model variants. [Colour figure can be viewed at [wileyonlinelibrary.com](https://onlinelibrary.wiley.com)]

The compression load reversal of Cycle 1 displays the stress distribution between the plastic zones caused by tension and compression,  $\omega_{FEM}^{tens.}$  and  $\omega_{FEM}^{compr.}$ . The corresponding triaxiality values of the FEM results display again a reduction in triaxiality surrounding the compressive plastic boundary with an opposite increase in  $\eta$  after the tensile plastic boundary. This behavior is also seen in the last tensile load reversal, where the gradual reduction in applied loads following the overload gives rise to seemingly erratic distributions of  $\eta$  and  $\sigma_{yy}$ .

Figure 8 presents the relative errors to FEM of the  $\sigma_{yy}(x)$  distributions at the first and last tensile load reversals. In addition to the Neuber model variants, the figure also shows the result of using the ‘exact’ FEM  $\sigma_{eq}(x)$  values in Hencky’s rule. The  $\sigma_{eq}(x)$  values from the same elasto-plastic FEM simulation to which errors are compared are extracted. These values are transformed to  $\sigma_{yy}(x)$  quantities using Hencky’s rule with the same elastic  $\sigma_{xx}/\sigma_{yy}$  values as used in the Neuber models. This highlights the error arising from the use of elastic triaxiality values. Figure 8 shows how stress correction gives good results for the first load reversal; however, the accuracy of the predictions deteriorates over time.

### 4.3 | VA Results—Cyclic Values

The cyclic quantities for select cycles as distributed over depth are shown in Figure 9. The figure shows the quantities relevant to the calculation of  $P_{SWT}$  quantities, as follows:

$$P_{SWT} = \sigma_{max} \cdot \epsilon_{amp} = (\sigma_{mean} + \sigma_{amp}) \cdot \epsilon_{amp}. \quad (25)$$

The crack-driving  $yy$ -components of the above cyclic quantities are inspected. The plastic boundary locations  $\omega$  in tension and compression obtained from FEM are shown for each cycle.

Figure 9 shows that both the stress and strain amplitudes are consistently predicted for each cycle. The differences become more significant with larger load magnitudes, but the shapes of the distributions remain similar. Mean stresses show larger differences for cycle 21, occurring after load levels have gradually been reduced from the main overload event of cycle 18. For the earlier cycles, the main trends are captured in all models although stress correction is slightly more beneficial in these instances.

### 4.4 | VA Results—Fatigue Damages

$P_{SWT}$  values are determined for each inspection point along the crack ligament line below the surface and their corresponding fatigue damages from each cycle of the VA load history are added up. Figure 10 shows the predicted accumulated damages  $D_{sum}^p(x)$  of each point below the notch root. Damage values are normalized to the maximum damage obtained from FEM,  $\max(D_{sum}^{FEM})$ , that is, the damage at the root. Different  $r_{RVE}$  sizes are also shown in the figure for reference, as well as

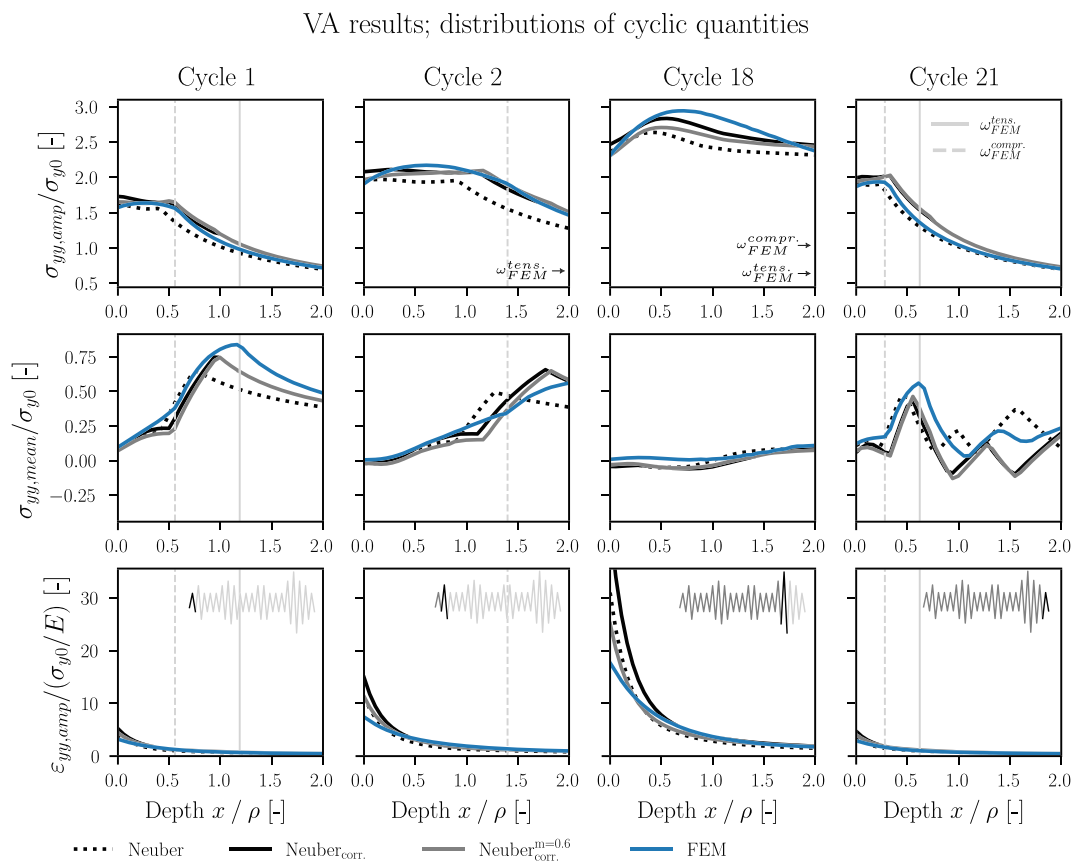


**FIGURE 9** | Stress and strain amplitudes and mean stress as distributed over depth for select load cycles of the VA simulation. Vertical gray lines indicate plastic boundaries  $\omega$  obtained from FEM for tensile and compressive load reversals. Plastic boundaries for cycles 2 and 18 exceed the  $x$ -limits shown. [Colour figure can be viewed at [wileyonlinelibrary.com](https://onlinelibrary.wiley.com)]

plastic zone sizes in tension for select load cycles,  $\omega_{FEM}^{nom}$  corresponding to a “nominal” cycle (cycle 1), and  $\omega_{FEM}^{OL}$  to the main overload event of cycle 18. The  $r_{RVE} = 30 \mu\text{m}$  size is not shown as the damage values have already reduced by 2 orders of magnitude after  $10 \mu\text{m}$ .

Results for the noncorrected Neuber’s rule show how it gives nonconservative damage values after  $x/\rho \approx 0.2$ , while stress correction causes damage predictions to be more conservative nearer to the root. Similar observations apply to ESED rule results.

Finally, Table 4 shows predicted averaged damage values compared with respective FEM values,  $D_{avg}^p/D_{avg}^{FEM}$ , when averaged over the different  $r_{RVE}$  sizes of 2, 10, and  $30 \mu\text{m}$ . Values above 1.0 indicate conservative life estimates relative to FEM, while values below 1.0 are nonconservative. When averaging the damage values obtained from Neuber’s rule without stress correction, the conservativeness at the root is balanced by the subsequent nonconservativeness below the root, although it is close to becoming nonconservative for the  $r_{RVE} = 30 \mu\text{m}$  case. When applying stress redistribution correction, the averaged values become significantly conservative due to higher predicted strain amplitudes. The ESED rule with stress correction performs well with the current sharp notch geometry. Using stress correction with the modified Neuber’s rule (Equation (4)) with  $m = 0.6$  flattens the errors of the stress and strain fields compared to FEM, giving slightly improved predictions and consistently conservative averaged damage values.

## 4.5 | Results Discussion

In the crack propagation models employing nonlocal continuum damage mechanics (see, e.g., Remes et al. [5] and Mikheevskiy and Glinka [6]), the stress and strain fields are used to determine the fatigue damage corresponding to fatigue crack growth. After enough damage has accumulated within the representative volume element, the crack is propagated by advancing the crack front. It is therefore important to correctly capture the distribution of stress and strain below a notch root.

When stress redistribution correction is used, the general trends of the stress distributions are captured with approximation rules, although the mean stresses well beyond the plastic boundary,  $\omega$ , become increasingly wrong over a VA simulation. However, in this case, when looking at averaged damages using the  $P_{SWT}$  quantity for a sharp notch, the error beyond  $\omega$  is secondary to the error closer to the root. This can also be seen in Figure 10 by looking at the markers  $\omega_{FEM}^{nom}$  for the size of the plastic boundary of a “nominal” load cycle and  $\omega_{FEM}^{OL}$  for the largest load peak of  $S = 0.7\sigma_{y0}$ . Most of the accumulated damage is concentrated between  $0 < x < 1\rho$ . The behavior between  $0 < x < \omega$  is consistent from cycle to cycle and can be studied by looking at a constant-amplitude loading case. VA loading, meanwhile, influences the results beyond  $\omega$  as the triaxiality, and mean stresses are seen to vary between FEM and the studied models.

When using stress correction, the overestimation of strain amplitudes is expected as finding the “correct” value for  $\omega$  essentially amplifies the pseudo-elastic stresses. Results become more

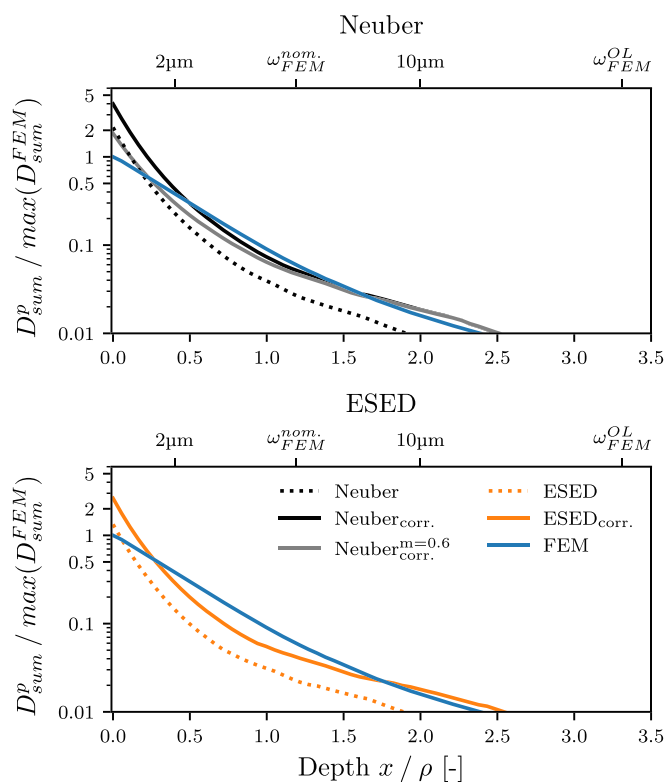


**FIGURE 10** | Distribution of predicted accumulated damage values  $D_{sum}^p$  for each inspection point. Values are normalized by the maximum scalar value obtained from FEM (i.e., the FEM-obtained damage value at the root). [Colour figure can be viewed at [wileyonlinelibrary.com](https://onlinelibrary.wiley.com)]

**TABLE 4** | Ratios of predicted average damages to values given by FEM,  $D_{avg}^p/D_{avg}^{FEM}$ , when using Equation (24) to obtain average damages.

$r_{RVE}$	Neuber	Neuber <sub>corr.</sub>	Neuber <sub>corr.</sub> <sup>m=0.6</sup>	ESED	ESED <sub>corr.</sub>
2 $\mu\text{m}$	1.29	2.39	1.27	0.8	1.58
10 $\mu\text{m}$	1.01	1.89	1.09	0.64	1.27
30 $\mu\text{m}$	1.0	1.86	1.09	0.64	1.26

Note: Values above 1.0 imply conservative life estimates compared to FEM and vice versa.

balanced when this is accounted for by modifying the approximation rule, such as the modified Neuber's rule (Equation (4)); see Figure 10 and Table 4. To estimate the optimal value of  $m$ , no directions are given by Stephens et al. [12]. Nonetheless, it is possible that a prediction made at the root with another model can be used to "calibrate" the  $m$  parameter to determine the field response. Neuber's rule without stress correction ( $m = 1$ ) is one example of this since it reliably gives conservative results at the root [25].

The results of this study indicate that stress redistribution correction improves stress field predictions under VA loading. However, the increased strain energy surrounding the root must be controlled via, for example, an alternative approximation rule in order for damage values to be correctly estimated. The framework studied under VA loading needs to be implemented in a crack growth model to assess the effect of the steps taken here on predictions of component failure. The effect of the  $m$ -parameter also needs to be evaluated for different geometries and load cases to understand its behavior and effect on results.

## 5 | Conclusions

In this study, the applicability of the classical plasticity approximation rules for nonlocal continuum damage-based crack growth modeling under variable-amplitude loading was investigated. Focus was placed on evaluating the performance of Neuber's rule [18] and Molski and Glinka's ESED rule [19] below the root of a notch. The combined hardening constitutive model of V-C was used to determine the material response at every load reversal during cyclic loading. A calculation framework was presented that determines the elasto-plastic response below a notch under variable-amplitude loading, accounting also for notch stress redistribution under plasticity. The resulting stress and strain fields were evaluated, and their combined effect on the distribution of fatigue damage in the material as well as the averaged damage values were compared to FEM results. The main findings are as follows:

1. Using stress redistribution correction, stresses were consistently predicted from cycle to cycle for both Neuber's and ESED rules.
2. When stress redistribution correction was applied, the predicted strains at the root became more conservative with both Neuber's and ESED rules, with a maximum error of approximately 100% at the notch root. This increased strain impacted fatigue damage values and caused significant

error in damage values. A modified Neuber's rule, including stress and strain constraint correction, successfully counteracts this.

3. While point-wise stresses and strains were not well-predicted below the notch root due to local variations induced by plasticity, averaged damages were conservative by approximately 30% at most compared to FEM, using a modified Neuber's rule.
4. Considering the obtained accuracy of the introduced computational framework, it shows good potential for giving quick engineering predictions of averaged damage values for crack growth analysis.

## Nomenclature

$\alpha$	Total backstress
$\alpha_k$	Backstress component $k$
$f_0$	Value of quantity at previous load reversal
$C_k$	Chaboche kinematic hardening parameter $C$ for backstress component $k$
$\gamma_k$	Chaboche kinematic hardening parameter $\gamma$ for backstress component $k$
$n_k$	Number of backstress components
$R$	Isotropic expansion
$Q$	Voce isotropic hardening parameter
$b$	Voce isotropic hardening parameter
$\kappa$	Sign of loading direction (1 or -1)
$t$	Current time/load step
$p$	Accumulated plastic strain
$a$	Notch depth
$\rho$	Notch root radius
$r_{RVE}$	Size of representative volume element
$d_{avg}$	Average grain size
$d_{99\%}$	Grain size at a probability level of 99%
$S$	Nominal stress
$E$	Elastic modulus
$\sigma_{y0}$	Nominal yield strength
$\nu$	Poisson's ratio
$\nu'$	Effective Poisson's ratio
$\sigma'_{f,cm}$	Coffin–Manson parameter
$b_{cm}$	Coffin–Manson parameter
$\epsilon'_{f,cm}$	Coffin–Manson parameter
$c_{cm}$	Coffin–Manson parameter
$m$	Parameter in modified Neuber relation
$K_t$	Elastic stress concentration factor
$K_{t,eq}$	Elastic equivalent stress concentration factor
$K_\sigma$	Plastic stress concentration factor
$K_\epsilon$	Plastic strain concentration factor

$\omega$	Plastic zone size
$\omega_0$	Plastic zone size predicted by linear pseudo-elastic stress field
$F_1, F_2$	Areas used in stress redistribution correction
$P_{SWT}$	Smith–Watson–Topper parameter
$N_f$	Load cycles to fatigue failure
$D$	Fatigue damage of one cycle
$D_{sum}$	Accumulated fatigue damage
$D_{avg}$	Averaged accumulated fatigue damage
$\eta$	Stress triaxiality
$s$	Pseudo-elastic stress
$e$	Pseudo-elastic total strain
$\sigma$	Actual elasto-plastic stress
$\varepsilon$	Actual elasto-plastic total strain
$\sigma_i, \varepsilon_i$	$i$ :th principal stress/strain component
$\sigma_{eq}, \varepsilon_{eq}$	Equivalent stress/strain
$\sigma_{amp}, \varepsilon_{amp}$	Amplitude of stress/strain over a load cycle
$\sigma_{mean}, \varepsilon_{mean}$	Mean of stress/strain over a load cycle
$\sigma_{max}, \varepsilon_{max}$	Maximum value of stress/strain over a load cycle
$\sigma_H$	Hydrostatic stress
$\varepsilon_e$	Elastic strain
$\varepsilon_p$	Plastic strain

#### Author Contributions

**Anton Asplund:** conceptualization, formal analysis, investigation, methodology, writing – original draft, writing – review and editing. **Heikki Remes:** conceptualization, funding acquisition, project administration, supervision, resources, writing – review and editing. **Yuki Ono:** supervision, writing – review and editing.

#### Acknowledgments

This research was funded by Aalto University and the CaNeLis project (funding from Business Finland under grant no. 3409/31/2022). The financial support is gratefully acknowledged.

#### Conflicts of Interest

The authors declare no conflicts of interest.

#### Data Availability Statement

Data will be made available upon request.

#### References

1. J. Aboudi, S. Arnold, and B. Bednarczyk, *Micromechanics of Composite Materials* (Butterworth-Heinemann, 2013).
2. S. Ghosh, K. Lee, and P. Raghavan, “A Multi-Level Computational Model for Multi-Scale Damage Analysis in Composite and Porous Materials,” *International Journal of Solids and Structures* 38, no. 14 (2001): 2335–2385.
3. M. G. D. Geers, V. G. Kouznetsova, and W. A. M. Brekelmans, “Multi-Scale Computational Homogenization: Trends and Challenges,” *Journal of Computational and Applied Mathematics* 234, no. 7 (2010): 2175–2182, Fourth International Conference on Advanced Computational Methods in Engineering (ACOMEN 2008).
4. J. Fish, G. Wagner, and S. Keten, “Mesoscopic and Multiscale Modeling in Materials,” *Nature Materials* 20 (2021): 774–786.
5. H. Remes, P. Varsta, and J. Romanoff, “Continuum Approach to Fatigue Crack Initiation and Propagation in Welded steel joints,” *International Journal of Fatigue* 40 (2012): 16–26.
6. S. Mikheevskiy, S. Bogdanov, and G. Glinka, “Analysis of Fatigue Crack Growth Under Spectrum Loading? The Unigrow Fatigue Crack Growth Model,” *Theoretical and Applied Fracture Mechanics* 79 (2015): 25–33.
7. H. Remes, P. Gallo, J. Jelovica, J. Romanoff, and P. Lehto, “Fatigue Strength Modelling of High-Performing Welded Joints,” *International Journal of Fatigue* 135 (2020): 105555.
8. W. Cui, F. Wang, and X. Huang, “A Unified Fatigue Life Prediction Method for Marine Structures,” *Marine Structures* 24, no. 2 (2011): 153–181.
9. J. R. Rice, “A Path Independent Integral and the Approximate Analysis of Strain Concentration by Notches and Cracks,” *Journal of Applied Mechanics* 35, no. 2 (1968): 379–386.
10. N. E. Dowling and J. A. Begley, “Fatigue Crack Growth During Gross Plasticity and the J-Integral,” *Mechanics of Crack Growth, ASTM STP 590* (1976): 82–103, <https://doi.org/10.1520/STP33940S>.
11. J. C. Newman, “A Crack-Closure Model for Predicting Fatigue-Crack Growth Under Aircraft Spectrum Loading,” 81941, NASA Technical Memorandum, (1981), <https://doi.org/10.1520/STP28334S>.
12. N. E. Dowling, “J-Integral Estimates for Cracks in Infinite Bodies,” *Engineering Fracture Mechanics* 26, no. 3 (1987): 333–348.
13. M. Vormwald and T. Seeger, “The Consequences of Short Crack Closure on Fatigue Crack Growth Under Variable Amplitude Loading,” *Fatigue and Fracture of Engineering Materials and Structures* 14 (1991): 205–225.
14. J. C. Newman, E. P. Phillips, and R. A. Everett, “Fatigue Analyses Under Constant- and Variable-Amplitude Loading Using Small-Crack Theory,” TM-1999-209329, NASA, (1999).
15. D. Radaj and M. Vormwald, *Advanced Methods of Fatigue Assessment* (Springer, 2013).
16. C. M. Davies, N. P. O'Dowd, K. M. Nikbin, G. A. Webster, and F. Biglari, “Comparison of Methods for Obtaining Crack-Tip Stress Distributions in an Elastic-Plastic Material,” *Journal of Strain Analysis for Engineering Design* 40 (2005): 431–449.
17. D. Taylor, “The Theory of Critical Distances,” *Engineering Fracture Mechanics* 75, no. 7 (2008): 1696–1705, Critical Distance Theories of Fracture.
18. H. Neuber, “Theory of Stress Concentration for Shear-Strained Prismatical Bodies With Arbitrary Nonlinear Stress-Strain Law,” *Journal of Applied Mechanics, Transactions ASME* 28 (1960): 544–550.
19. K. Molski and G. Glinka, “A Method of Elastic-Plastic Stress and Strain Calculation at a Notch Root,” *Materials Science and Engineering* 50 (1981): 93–100.
20. G. Glinka, “Energy Density Approach to Calculation of Inelastic Strain-Stress Near Notches and Cracks,” *Engineering Fracture Mechanics* 22 (1985): 485–508.
21. R. Stephens and H. Fuchs, *Metal Fatigue in Engineering* (John Wiley & Sons, 1980).
22. W. N. Sharpe and K. C. Wang, “EVALUATION of a Modified Monotonic Neuber Relation,” *Journal of Engineering Materials and Technology, Transactions ASME* 113 (1991): 1–8.
23. K. C. Wang and W. N. Sharpe, “EVALUATION of a Modified Cyclic Neuber Relation,” *Journal of Engineering Materials and Technology, Transactions ASME* 113 (1991): 350–353.
24. C. H. Wang and L. R. F. Rose, “Transient and Steady-State Deformation at Notch Root Under Cyclic Loading,” *Mechanics of Materials* 30 (1998): 229–241.
25. M. Knop, R. Jones, L. Molent, and C. Wang, “On the Glinka and Neuber Methods for Calculating Notch Tip Strains Under Cyclic Load Spectra,” *International Journal of Fatigue* 22 (2000): 743–755.

26. S. Kilambi and S. M. Tipton, "Numerical Evaluation of the Original "Neuber's Rule" for Pure Out-of-Plane Shear Loading," *Journal of Strain Analysis for Engineering Design* 48 (2013): 522–535.
27. C. H. Wang, W. Guo, and L. R. F. Rose, "A Method for Determining the Elastic-Plastic Response Ahead of a Notch Tip," *Journal of Engineering Materials and Technology, Transactions ASME* 121 (1999): 313–320.
28. A. Ince and G. Glinka, "Approximation Modeling Framework for Elastic-Plastic Stress-Strain Fields Near Cracks With a Small Finite Crack Tip Radius," *Theoretical and Applied Fracture Mechanics* 121 (2022): 103452.
29. J. L. Chaboche, P. Kanouté, and F. Azzouz, "Cyclic Inelastic Constitutive Equations and Their Impact on the Fatigue Life Predictions," *International Journal of Plasticity* 35 (2012): 44–66.
30. M. Skorupa, "Load Interaction Effects During Fatigue Crack Growth Under Variable Amplitude Loading - A Literature Review. Part I: Empirical Trends," *Fatigue & Fracture of Engineering Materials & Structures* 21, no. 8 (1998): 987–1006.
31. M. Hoffmann and T. Seeger, "A Generalized Method for Estimating Multiaxial Elastic-Plastic Notch Stresses and Strains Part 1: Theory," *Journal of Engineering Materials and Technology, Transactions ASME* 107 (1985): 250–254.
32. M. Hoffmann and T. Seeger, "A Generalized Method for Estimating Multiaxial Elastic-Plastic Notch Stresses and Strains Part 2: Application and General Discussion," *Journal of Engineering Materials and Technology, Transactions ASME* 107 (1985): 255–260.
33. W. F. Chen and D. J. Han, *Plasticity for Structural Engineers* (Springer, 1988).
34. N. E. Dowling, *Mechanical Behavior of Materials* (Pearson, 2013).
35. A. R. Hartloper, A. de Castro e Sousa, and D. G. Lignos, "Constitutive Modeling of Structural Steels: Nonlinear Isotropic/Kinematic Hardening Material Model and Its Calibration," *Journal of Structural Engineering* 147 (2021): 4021031.
36. A. Petry, "Nonlinear Material Modelling for Fatigue Life Prediction of Welded Joints in High Strength Marine Structures," (Master's Thesis, Espoo, Finland, 2022).
37. M. Creager and P. Paris, "Elastic Field Equations for Blunt Cracks With Reference to Stress Corrosion Cracking," *International Journal of Fracture Mechanics* 3 (1967): 247–252.
38. G. Glinka, "Calculation of Inelastic Notch-Tip Strain-Stress Histories Under Cyclic Loading," *Engineering Fracture Mechanics* 22 (1985): 839–854.
39. ASTM, "Standard Practices for Cycle Counting in Fatigue Analysis - ASTM Standard e1049-85(2023)," (2023).